Applied Mathematical Modelling 37 (2013) 284–307

Contents lists available at SciVerse ScienceDirect

Applied Mathematical Modelling

journal homepage: www.elsevier.com/locate/apm

Numerical simulation of vortex induced vibrations and its control by suction and blowing

K. Muralidharan, Sridhar Muddada, B.S.V. Patnaik *

Fluid Mechanics Laboratory, Department of Applied Mechanics, Indian Institute of Technology Madras, Chennai 600 036, India

ARTICLE INFO

Article history:
Received 21 August 2011
Received in revised form 21 November 2011
Accepted 15 February 2012
Available online 3 March 2012

Keywords:
Active flow control
Flow induced vibrations
Fluid structure interaction
CFD

ABSTRACT

The vortex formation and shedding behind bluff structures is influenced by fluid flow parameters such as, Reynolds number, surface roughness, turbulence level, etc. and structural parameters such as, mass ratio, frequency ratio, damping ratio, etc. When a structure is flexibly mounted, the Kármán vortex street formed behind the structure gives rise to vortex induced oscillations. The control of these flow induced vibrations is of paramount practical importance for a wide range of designs. An analysis of flow patterns behind these structures would enable better understanding of wake properties and their control. In the present study, flow past a smooth circular cylinder is numerically simulated by coupling the mass, momentum conservation equations along with a dynamical evolution equation for the structure. An active flow control strategy based on zero net mass injection is designed and implemented to assess its efficacy. A three actuator system in the form of suction and blowing slots are positioned on the cylinder surface. A single blowing slot is located on the leeward side of the cylinder, while two suction slots are positioned at an angle $\alpha = 100^{\circ}$. This system is found to effectively annihilate the vortex induced oscillations, when the quantum of actuations is about three times the free stream velocity. The dynamic adaptability of the proposed control strategy and its ability to suppress vortex induced oscillations is verified. The exact quantum of actuation involved in wake control is achieved by integrating a control equation to decide the actuator response in the form of a closed loop feed back system. Simulations are extended to high Reynolds number flows by employing eddy viscosity based turbulence models. The three actuator system is found to effectively suppress vortex induced oscillations.

1. Introduction

Fluid flow past a circular cylinder is a model problem of fundamental interest, as it impacts a number of practical engineering applications. Vortices are formed and shed behind bluff bodies causing a sinuous wake in its downstream. Alternating eddies formed behind a bluff object gives rise to fluctuating lift and drag forces. Hence, the problem of flow past a circular cylinder and its wake control is of interest to a variety of design practitioners who are affected by vortex induced oscillations such as, bridges, skyscrapers, offshore structures, marine cables, submarines, etc. [1].

The fluctuating force field exerted by the fluid on the structure, causes it to deform if rigidly mounted or oscillate if it is flexibly mounted. When the structure oscillates or undergoes deformations, its orientation to the flow and in turn, the fluid forces acting on it changes. The governing equations for such a system are, the mass and momentum conservation for the

* Corresponding author.
E-mail address: bsvp@iitm.ac.in (B.S.V. Patnaik).

0307-904X/$ - see front matter © 2012 Elsevier Inc. All rights reserved.
doi:10.1016/j.apm.2012.02.028

fluid, and an additional equation that would describe the dynamical motion of the structure. Thus the study of vortex induced vibration (VIV) involves a two way coupling between the dynamical equations that govern both the fluid and the structure [2]. A number of recent and critically acclaimed reviews on diverse aspects of flow induced oscillations are available in the literature (see references [3–5]).

The problem of flow past vibrating bodies can be tackled in two fundamentally different ways, which perhaps complement each other. The first approach is the study of forced vibrations, where an external excitation is imparted to the rigid body and then its effect on the flow field is investigated [6–8]. Here, the frequency and amplitude combination for the oscillations can be chosen at will and imposed on the circular cylinder, to study the effect of an oscillating bluff body in a fluid stream. The second approach involves study of free vibrations, where the fluctuating temporal lift force induces the body to oscillate. This would generate the necessary coupling between the structure and the flow field, to result in the evolution of cylinder displacements.

Feng [9] contributed to some of the landmark experimental measurements of structural response for an elastically mounted cylinder. He measured quantities such as, amplitude of cylinder vibration (y), vibration frequency (f_v) and phase difference (ϕ) between force and displacement, etc. These quantities were plotted against normalized velocity ($v_r = u/f_n D$). Two distinct amplitude branches, namely the 'initial' branch and the 'lower' branch, were observed with a jump in response amplitude, with a significant jump in the phase of the pressure fluctuations relative to body motion. A jump in phase angle between transverse force and displacement under resonance, is typically matched by a switch in the timing of vortex shedding. Williamson and Roshko [8] have associated this jump to a shift from 2S vortex shedding mode to 2P mode. Here 2S refers to shedding of two alternating eddies, while 2P refers to two pairs of eddies being shed on each side of the cylinder. Anagnostopoulos and Bearman [10] have performed 1-DOF experiments and captured the *lock-in* range and the phenomenon of beating for pure laminar vortex shedding range $Re \approx 90 - 150$. One of the first successful attempts to numerically simulate flow past a vibrating body has employed Marker and cell (MAC) method [11]. Chilukuri [12] has improved the predictions of Hurlbut et al. [11] by using simplified MAC approach (SMAC). Patnaik et al. [13] have used Galerkin based finite element method to capture the synchronization regime and associated wake patterns. Meneghini and Bearman [14] have used a discrete vortex method (DVM) with a vortex in cell (VIC) procedure by incorporating viscous diffusion. They have demonstrated that 2S mode persists up to $A/D = 0.6$ and beyond which $P + S$ type wake pattern was found to prevail. Zhou et al. [15] have analyzed the cylinder response, damping, forces induced, etc. employing discrete vortex simulations. Leontini et al. [16] have performed experiments to determine if forced oscillations were consistent with self excited oscillations. Although similarities were seen, considerable sensitivity to input forcing was noticed. Khalak and Williamson [17] carried out free vibration studies with low mass damping and obtained a response pattern markedly different from Feng's [9] findings. Among the analytical approaches, Bishop and Hassan [7] were the first to model vortex shedding as a non-linear fluid oscillator and coupled it to the structural oscillator.

The rapid advances in materials, is making the structures more flexible and lighter, this necessitates analysis of vortex induced vibrations. Therefore the ability to manipulate and control the flow field to reduce flow induced oscillations is gaining importance. Control of these vibrations can be attained by modifying the fluid forces responsible for oscillation, either through active or passive means. Active closed loop control naturally lends itself to feedback mechanism and changes in upstream conditions. However, passive strategies such as helical strakes, shrouds, slats, splitter plates, etc. do not require additional energy expenditure [18]. A wide variety of other active and passive control strategies have been reported in the literature [19]. Recently, Baek and Karniadakis [20] have introduced a slit along the streamwise direction, which passes through the cylinder to create a jet that interacts with the wake to suppress vortex shedding. Chen and Aubry [21] have developed a closed loop algorithm to suppress vortex induced vibrations by means of direct numerical simulations (DNS). They have used Lorentz forces to control the cylinder oscillations based on partial flow information available on the surface of the cylinder. However, in practical applications, blowing and suction [22], accoustic acutations [23] and cylinder rotations [24] are some of the widely known active flow control techniques. Inspired by the pioneering work on chaos control by OGY [25], Patnaik and Wei [26] have proposed the stabilization of unstable periodic orbits (UPO) through synchronization based coupling between driver system and target system. By this coupling, complete annihilation of wake vortices behind a D-cylinder was achieved. The strategy of momentum injection control was further extended by Muddada and Patnaik [27] to control vortex shedding behind a circular cylinder by means of two symmetric rotating elements.

Although some of the attempts mentioned above, are only theoretical in nature, the need to control VIV is of concern to practicing engineers. In the present study, we investigate the influence of vortex induced vibrations on the Kármán vortex street, and the resulting modifications on the wake zone. To start with, the self excited nature of the oscillations are allowed to be generated. We then, investigate the influence of suction and blowing in controlling these self-excited oscillations. To this end, the following objectives have been framed:

- To validate the influence of forced cylinder oscillations on the vortex structures behind a circular cylinder by generating different wake modes such as 2S, 2P, and $P + S$ for different excitation frequency and amplitude combinations.
- To investigate free vibrations by coupling equation of structure with the equations governing the fluid flow.
- To study the response of the circular structure under the active flow control strategy of suction and blowing. Further more, to investigate the efficacy and dynamic adaptability of suction and blowing on the self excited oscillations.
- To study the effectiveness of blowing and suction for high Reynolds number turbulent wakes.

2. Governing equations and solution methodology

2.1. Effect of structural oscillations

The study of vortex induced vibrations entails the computation of forces for flow past a cylinder and track its temporal evolution. This in turn necessitates calculation of the cylinder displacement which is triggered by the fluctuating lift force acting on the structure. The support on which the cylinder is mounted, is assumed to be flexible with linear spring stiffness that enable smooth periodic oscillations. The most common model used to describe the motion of the structure is through the idealizations involving mass, spring and damper system. The schematic shown in Fig. 1(a), depicts a one degree of freedom system. Motion is enabled only along the y-direction by virtue of its connectivity to linear springs. The cylinder is assumed to be rigid, and thus only the position of the center of gravity (for that matter any reference point on the cylinder) can be tracked as a function of time. The acceleration produced by the structure is due to balance of forces such as, elastic restoration force, damping force. Over and above this, forces generated by the fluid on the cylinder along its direction of motion needs to be taken into account.

The governing equation for the structure is given by

$$m\ddot{y} + c\dot{y} + ky = F_L(t), \tag{1}$$

where $F_L(t)$ refers to the fluctuating lift force. The parameters associated with the structure, viz., mass (m), damping (c) and stiffness (k), are chosen inline with earlier experimental studies. Once the lift force is determined by solving the Navier–Stokes equations, the ordinary differential Eq. (1) can be solved to find the position of the cylinder.

Since the fluid flow equations are discretized, $F_L(t)$ is not available as a continuous function but as an instantaneous value at the end of every time step. Ideally the equation of the structure should be solved at the same temporal level at which fluid force is obtained. Nevertheless, a second order accurate discretization is carriedout with an explicit formulation as follows:

$$m\left(\frac{y^{n+1} - 2y^n + y^{n-1}}{(\Delta t)^2}\right) + c\left(\frac{y^{n+1} - y^{n-1}}{2(\Delta t)}\right) + k(y^n) = F_L^n. \tag{2}$$

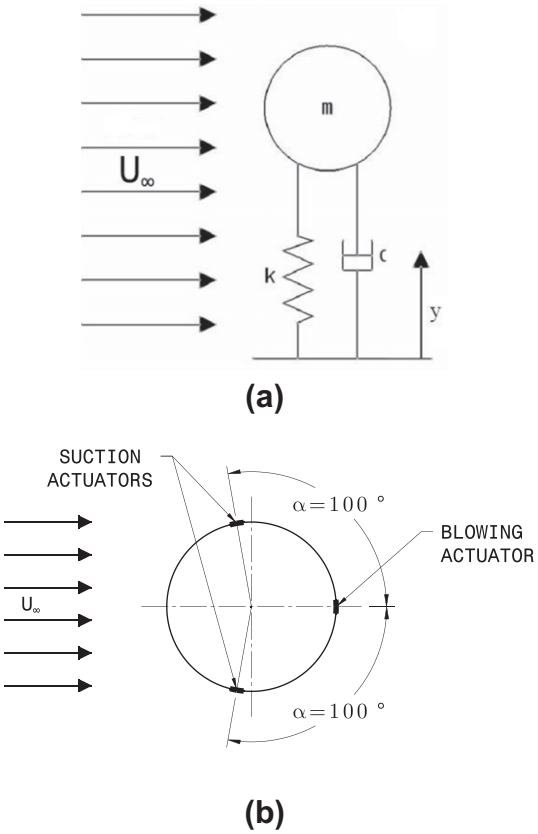

Fig. 1. (a) A single degree of freedom (SDOF) model for vortex induced vibrations, (b) close-up view of three actuator system (the locations of suction and blowing slots indicated in the figure).

The above equation, can be rearranged as:

$$y^{n+1}\left(\frac{m}{(\Delta t)^2}+\frac{c}{2(\Delta t)}\right)=F_L^n+y^n\left(\frac{2m}{(\Delta t)^2}-k\right)+y^{n-1}\left(\frac{c}{2(\Delta t)}-\frac{m}{(\Delta t)^2}\right). \tag{3}$$

Eq. (3) can be further simplified as:

$$y^{n+1}=\frac{F_L^n}{C_1}+y^n\frac{C_2}{C_1}+y^{n-1}\frac{C_3}{C_1}, \tag{4}$$

where C_1, C_2, C_3 constants are shown in parenthesis of Eq. (3).

At the end of each time step, lift force on the structure is obtained from the flow solver. The current position of the centre of gravity of the cylinder is updated and its position at the next time step is obtained. The values of m, c and k employed in the present investigation are 1.0, 0.0016 and 0.66, respectively. However, in the present simulations, m is kept constant, while natural frequency (f_n) variation is obtained by changing the spring stiffness (k).

2.2. Fluid flow model

The fluid flow is assumed to be incompressible, Newtonian and two-dimensional. In the context of wake behind a cylinder, three-dimensionality effects set in around $Re \approx 200$ [28]. For high Reynolds number turbulent flows, resorting to statistical averaging techniques is the preferred choice. To this end, Reynolds averaging is performed on the instantaneous mass, momentum conservation equations. The unsteady Reynolds averaged Navier–Stokes (URANS) version of equations are given as:

$$\frac{\partial \bar{u}_i}{\partial x_i}=0, \tag{5}$$

$$\frac{\partial \bar{u}_i}{\partial t}+\bar{u}_j\frac{\partial \bar{u}_i}{\partial x_j}=-\frac{1}{\rho}\frac{\partial \bar{p}}{\partial x_i}+\frac{\partial\left(\bar{\tau}_{ij}+\tau_{ij}^R\right)}{\partial x_j}. \tag{6}$$

where

$$\tau_{ij}^R=-\rho\overline{u_i'u_j'};\quad \bar{\tau}_{ij}=\frac{\mu}{\rho}\left(\frac{\partial \bar{u}_i}{\partial x_j}+\frac{\partial \bar{u}_j}{\partial x_i}\right). \tag{7}$$

Here, τ_{ij}^R and $\bar{\tau}_{ij}$ are the Reynolds stress and mean shear stress tensors respectively. For high Re flows, τ_{ij}^R need to be suitably approximated through closure modelling strategies. However, when simulations are performed for low Re range, τ_{ij}^R is set to zero and additional equations need not be invoked as it simplifies to a non-statistical approach. All geometrical length scales are normalized with the size of cylinder diameter (D), streamwise and cross stream velocities with the inlet velocity (U_∞), physical time (t) with $\left(\frac{D}{U_\infty}\right)$, and pressure (p) with (ρU_∞^2), where ρ refers to the fluid density. The flow domain of interest is shown in Fig. 2, where all the dimensions indicated are based on the cylinder diameter D. The overall size of the domain is 32D in the streamwise direction and 16D along the cross-streamwise direction. The centre of the cylinder is 8D from the left boundary. The left boundary is imposed with *velocity inlet* boundary condition, where u, is specified as U_∞ and $v=0$. The right boundary is assigned with an *outflow* boundary condition with normal gradients $\frac{\partial u}{\partial x}$ and $\frac{\partial v}{\partial x}$ set to zero. The upper and

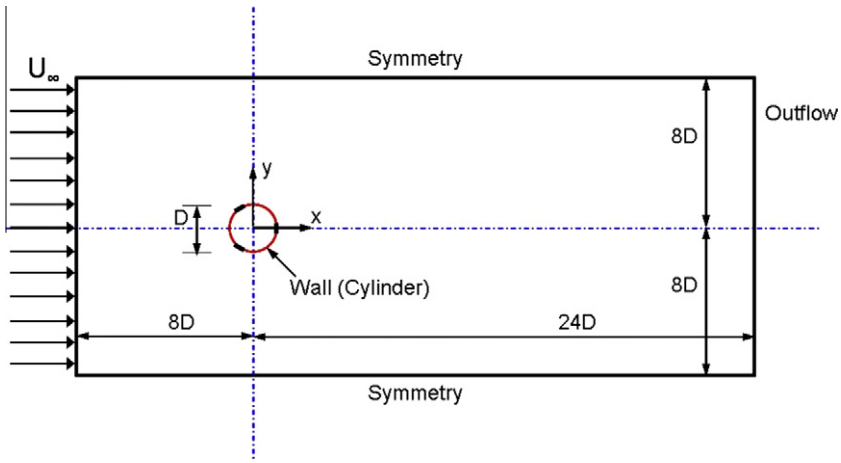

Fig. 2. Flow domain of interest with boundary conditions. 'D' and 'U_∞' represent the diameter of the circular cylinder and freestream velocity, respectively.

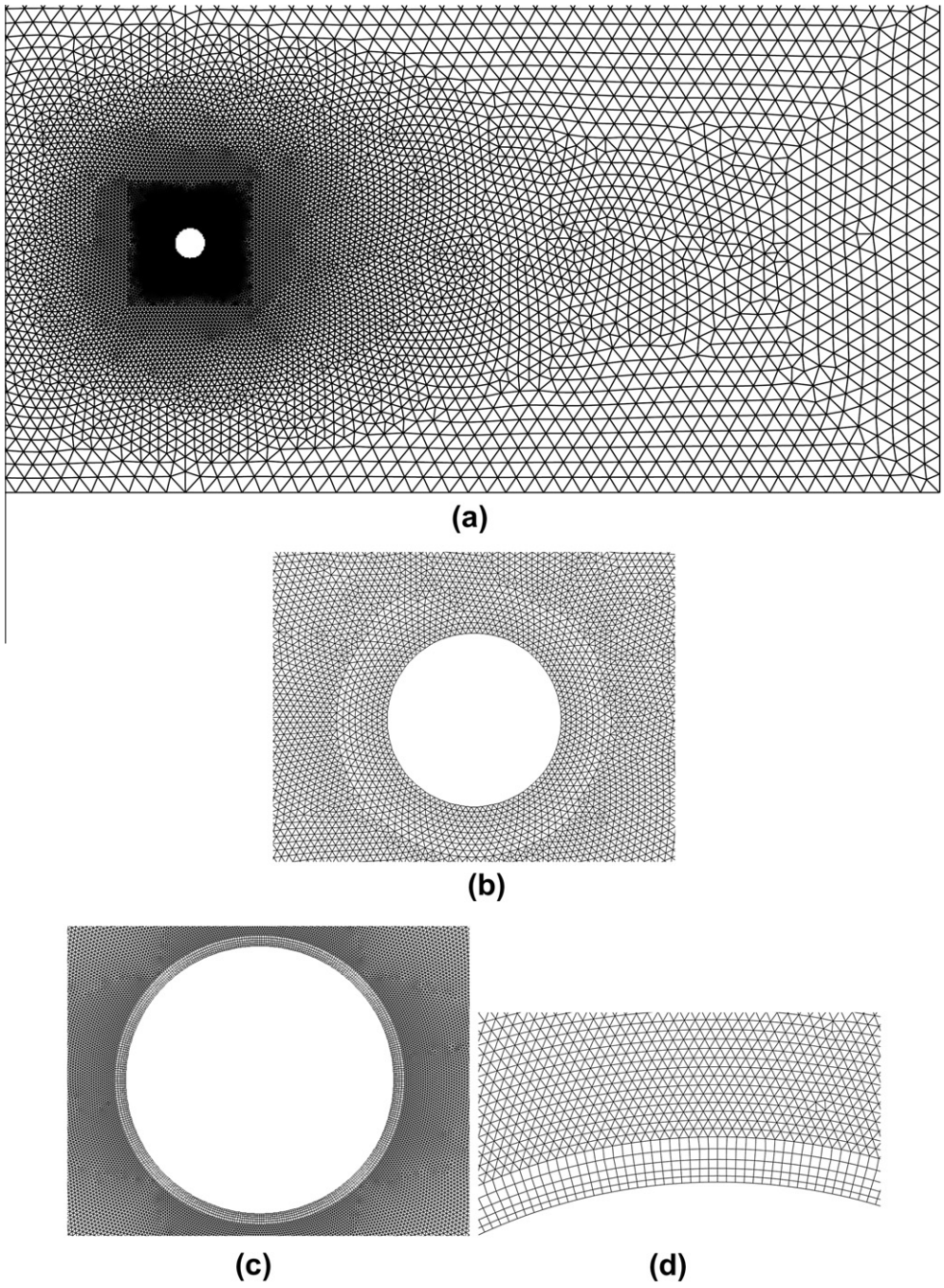

Fig. 3. Mesh used and comparison of a tri grid (A/B/C) with hybrid grid (D). (a) Typical mesh used, (b) tri grid, (c) hybrid grid, (d) close-up view of hybrid grid.

lower boundaries are assigned with *symmetry* boundary condition $\left(\frac{\partial u}{\partial y} = 0; v = 0\right)$. The cylinder surface is assigned a no-slip *wall* $(u = v = 0)$ boundary condition. The flow through the suction and blowing slots are assigned zero tangential velocity but with a specified normal velocity as dictated by the actuator response from the control algorithm.

The popular finite volume based SIMPLE family of schemes [29], which is incorporated in FLUENT [30] is used in our numerical calculations. A second order accurate semi-implicit scheme is chosen for the time integration. The spatial discretization is performed on a standard collocated grid using finite volume method. In the Semi-Implicit Pressure Linked Equation (SIMPLE) solver, the pressure gradient is treated implicitly at $(n + 1)$th, time level, while all other terms are explicitly treated at (n)th time level. The practical implementation of the scheme is achieved through the computation of intermediate

velocities. Subsequently, in the velocity correction phase, these values are projected into the divergence free vector space and corrected. However, ahead of the velocity correction phase, the following, Poisson equation needs to be solved:

$$\nabla^2 \bar{p}^{n+1} = -\frac{1}{\Delta t}\frac{\partial u_i^*}{\partial x_i} + \nabla^2 p^*. \tag{8}$$

Here, variables with $*$ indicate intermediate velocities and pressures. Further details related to the flow solver and spatial discretization are available in references [29,32]. As a precursor to the present investigation, numerical study of flow past a stationary cylinder is typically carried out using quadrilateral elements for meshing. Since the present study involves dynamic meshing to accommodate for the cylinder oscillations, a mesh with triangular elements is more amenable to quick changes (deformations) in elemental connectivity. Ideally, the whole domain of interest should be tessellated with triangular elements. Better resolution of the velocities and hence computation of the velocity gradients with in the boundary layer is better enabled through structured quadrilateral elements. Fig. 3 depicts the domain discretization with a close up view of the mesh near fluid–structure interaction region. Note in particular a fine mesh closer to no-slip boundaries encompassing the circular cylinder. The difference between a pure triangular grid and a hybrid grid is illustrated in Fig. 3(b)–(d).

2.3. Turbulence modeling

Navier–Stokes equations in their standard form are sufficient to resolve the wide spectrum of eddy scales by enabling a fine grid resolution. Such a route is popularly called direct numerical simulations (DNS). However, in DNS the computational expenditure shoots up approximately as Re^3 [33]. Therefore, statistical averaging, via URANS with the aid of standard two-equation turbulence models are popular in industrial practice. These models rely on turbulent eddy viscosity hypothesis which assumes a linear approximation between Reynolds stress tensor and the strain rate tensor. In the present investigation, Reynolds stresses $\overline{u_i' u_j'}$ are approximated by solving an evolution equation for turbulent kinetic energy (k) and its rate of dissipation (ϵ). The standard $k-\epsilon$ model of Launder and Spalding [35] uses the eddy viscosity hypothesis of Boussinesq:

$$\overline{u_i' u_j'} = \nu_t\left(\frac{\partial \bar{u}_i}{\partial x_j} + \frac{\partial \bar{u}_j}{\partial x_i}\right) - \frac{2}{3}k\delta_{ij}. \tag{9}$$

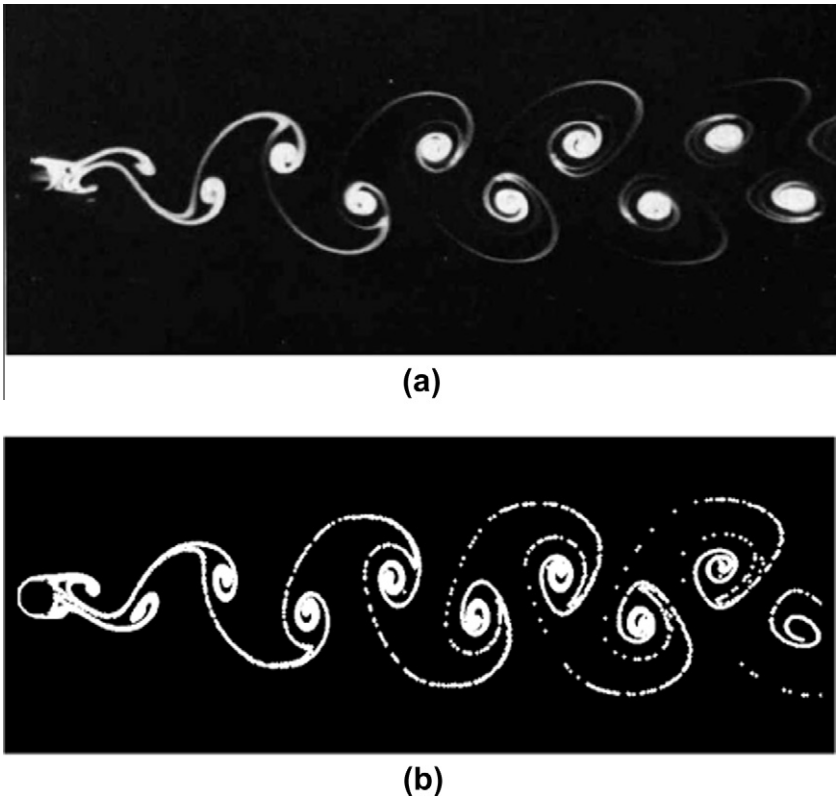

Fig. 4. Flow separation and vortex shedding behind a circular cylinder (a) $Re = 105$ [42] and (b) Present simulation ($Re = 100$).

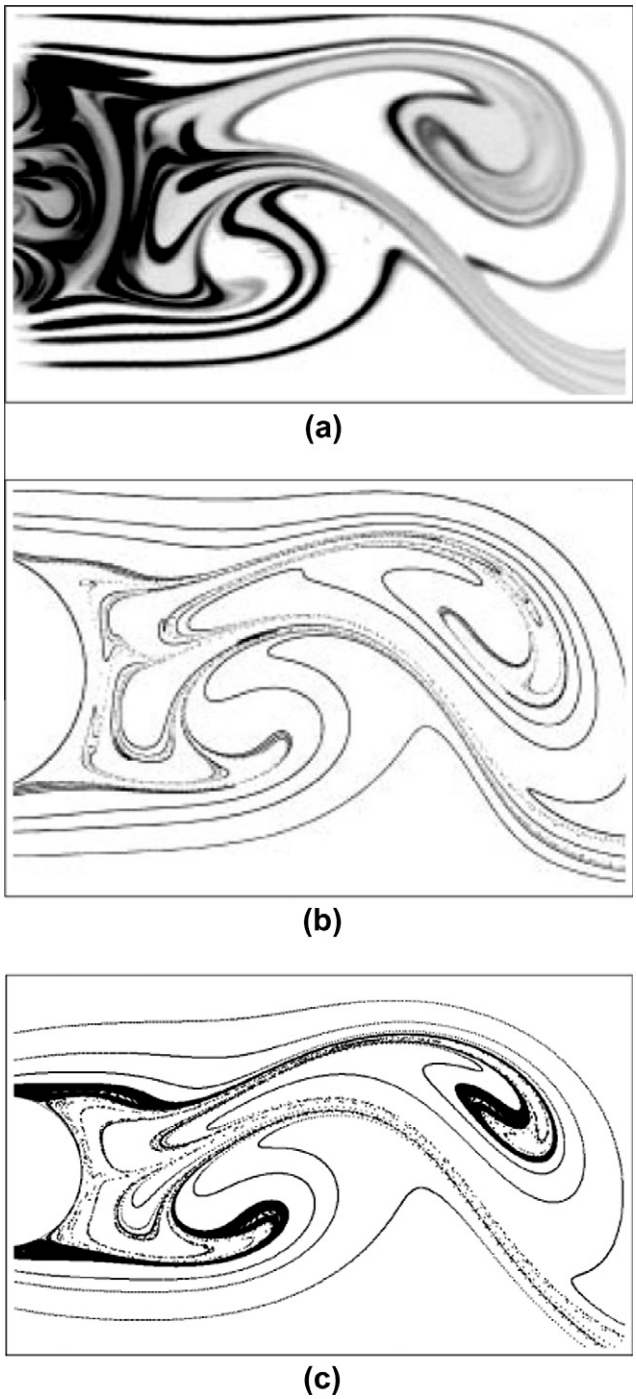

Fig. 5. Comparison of dynamics of the near wake, (a) Experimental [43], (b) Computed result [43] and (c) Presented study.

This concept works on the assumption that the Reynolds stresses are linearly related to the mean velocity gradients through a proportionality constant, given by the turbulent eddy viscosity v_t. In the $k-\epsilon$ model, the turbulent eddy viscosity is related to the turbulent kinetic energy (k) and to the rate of its dissipation (ϵ) as:

$$v_t = c_\mu \frac{k^2}{\epsilon}. \tag{10}$$

Table 1
Comparison of forces on the cylinder and Strouhal number for flow past a rigid circular cylinder at $Re = 100$.

S. No.	References	$\overline{C_d}$	$C_{l,rms}$	St
1	Engelman and Jamina [38]	1.40	0.257	0.170
2	Kang et al. [39]	1.34	0.236	0.164
3	Sharman et al. [40]	1.32	0.230	0.164
4	Burbeau and Sagaut [41]	1.41	0.257	0.164
5	Present study	1.41	0.242	0.167

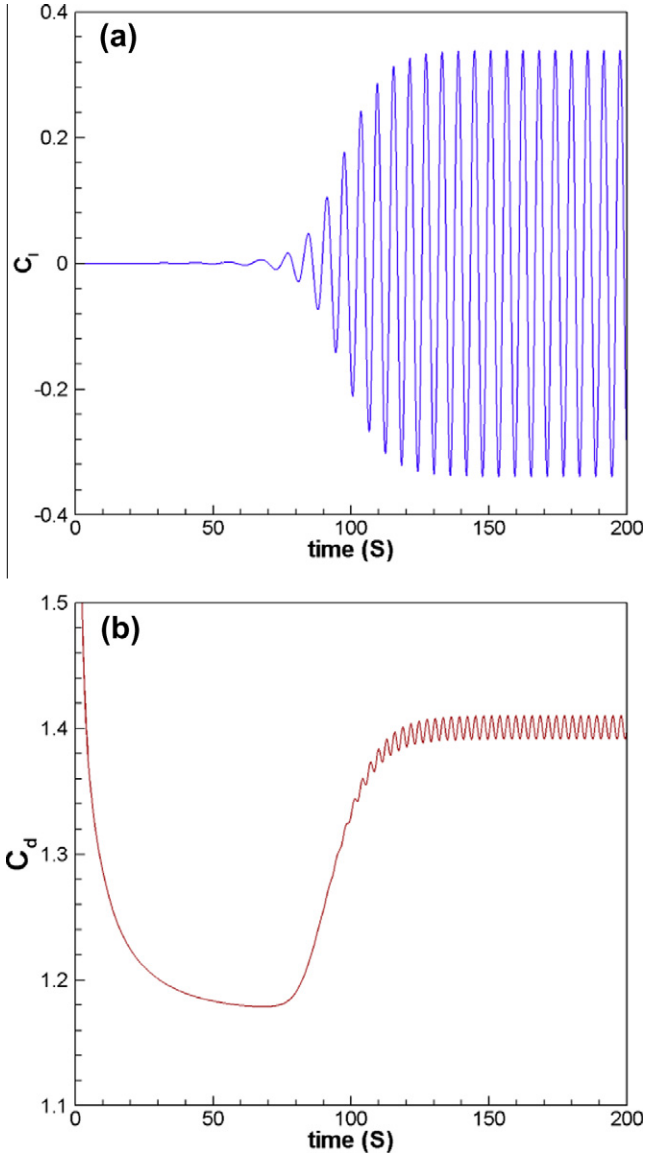

Fig. 6. Temporal history of (a) lift coefficient (C_l) and (b) drag coefficient (C_d) for flow past a rigid cylinder at $Re = 100$.

2.3.1. $k - \epsilon$ model [36]

The spatial and temporal distribution of k and ϵ is governed by the differential form of the transport equations for these quantities, considering the history and transport effects of turbulence:

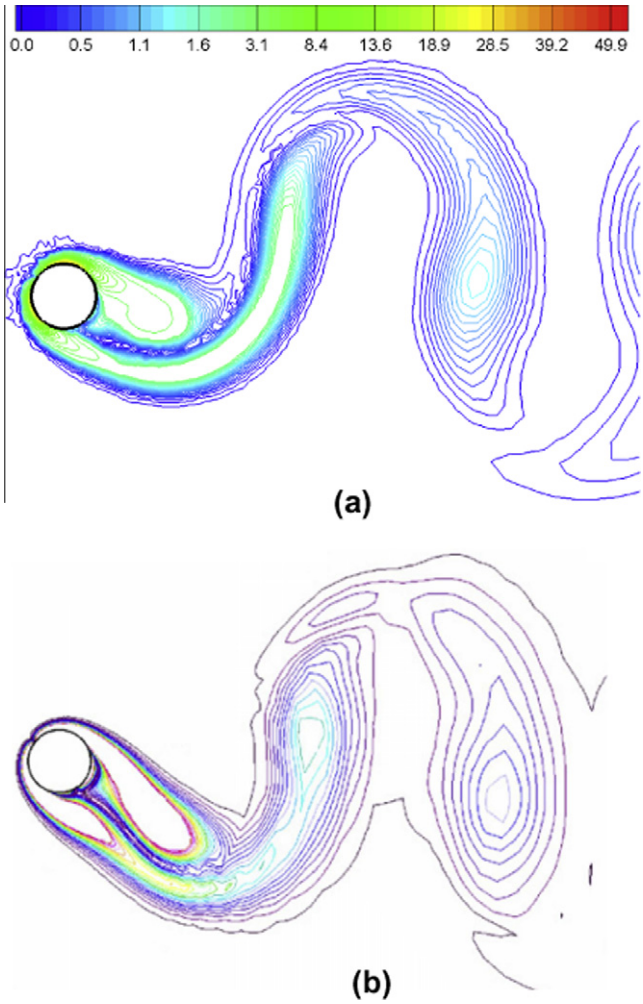

Fig. 7. Vorticity contours for flow past a vibrating cylinder, the presence a deformed 2*S* like vortex shedding mode can be noticed for $A^* = 1$ and $f^* = 0.9$. (a) Present study, (b) Placzek et al. [31].

$$\frac{\partial k}{\partial t} + \frac{\partial[\overline{u_l}k]}{\partial x_l} = \frac{\partial}{\partial x_l}\left(\left(\nu + \frac{\nu_t}{\sigma_k}\right)\frac{\partial k}{\partial x_l}\right) + P_k - \epsilon, \tag{11}$$

$$\frac{\partial \epsilon}{\partial t} + \frac{\partial[\overline{u_l}\epsilon]}{\partial x_l} = \frac{\partial}{\partial x_l}\left(\left(\nu + \frac{\nu_t}{\sigma_\epsilon}\right)\frac{\partial \epsilon}{\partial x_l}\right) + C_{\epsilon 1}P_k\frac{\epsilon}{k} - C_{\epsilon 2}\frac{\epsilon^2}{k}, \tag{12}$$

with P_k referring to production of turbulent kinetic energy, which is given as:

$$P_k = \nu_t S^2 \quad \text{where,} \quad S = \sqrt{\frac{1}{2}\left[\frac{\partial \bar{u}_i}{\partial x_j} + \frac{\partial \bar{u}_j}{\partial x_i}\right]^2}. \tag{13}$$

Here, S refers to the symmetric mean strain rate tensor. The model constants used in the above equations are: $c_\mu = 0.09$, $C_{\epsilon 1} = 1.44, C_{\epsilon 2} = 1.92, \sigma_k = 1.0$ and $\sigma_\epsilon = 1.3$.

2.3.2. $k - \epsilon$ model of Kato and Launder [34]

The standard $k - \epsilon$ model is modified by Kato and Launder to control and regulate the over production of the turbulent kinetic energy in the stagnation regions. Kato and Launder [34] introduced the following ad hoc model relation for the production term in the turbulent kinetic energy equation:

$$P_k = \nu_t S\Omega \quad \text{instead of} \quad P_k = \nu_t S^2. \tag{14}$$

The quantity Ω is an antisymmetric rotation tensor and is proportional to the magnitude of the local vorticity and is given as:

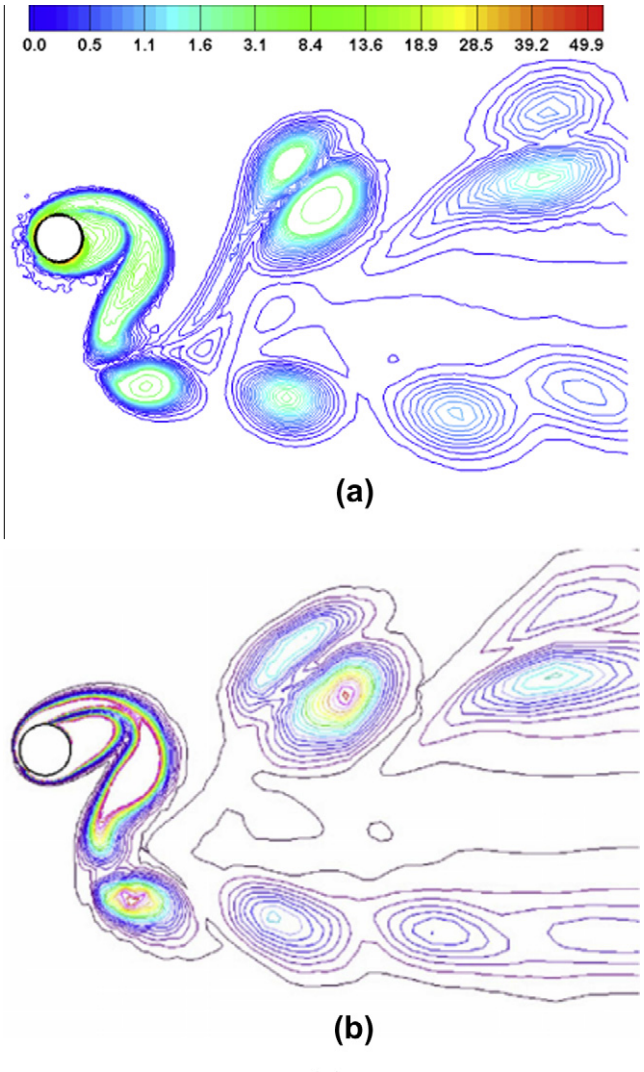

Fig. 8. Vorticity contours for flow past a vibrating cylinder, $P+S$ vortex shedding mode is noticed for $A^* = 1.25$ and $f^* = 1.5$. (a) Present study, (b) Placzek et al. [31].

$$\Omega = \sqrt{\frac{1}{2}\left[\frac{\partial \bar{u}_i}{\partial x_j} - \frac{\partial \bar{u}_j}{\partial x_i}\right]^2}; \quad S = \sqrt{\frac{1}{2}\left[\frac{\partial \bar{u}_i}{\partial x_j} + \frac{\partial \bar{u}_j}{\partial x_i}\right]^2}. \tag{15}$$

In simple shear flows, the behavior of the production term remains unchanged as $\Omega \approx S$, while spurious turbulence production is eliminated as $\Omega \approx 0$ in stagnation regions. Here, the model constants used are same as that in the standard $k-\epsilon$ model. However, these model constants need not be recalibrated owing to the fact that production term is identical both in standard $k-\epsilon$ and Kato and Launder's modification for simple shear flows.

3. Results and discussion

In this section, numerical simulation of flow past a circular cylinder with and without actuator controls are discussed. The influence of suction and blowing on the self excited cylinder oscillations is analyzed. The effect of turbulence and dynamic adaptability of the control technique are also investigated.

3.1. Kármán vortex shedding behind a circular cylinder

Before we proceed to study the flow past a vibrating body, it is necessary to validate the dynamics of the vortex structures past a rigid cylinder. The spatio-temporal features of the wake zone is best reflected through the streakline visuals.

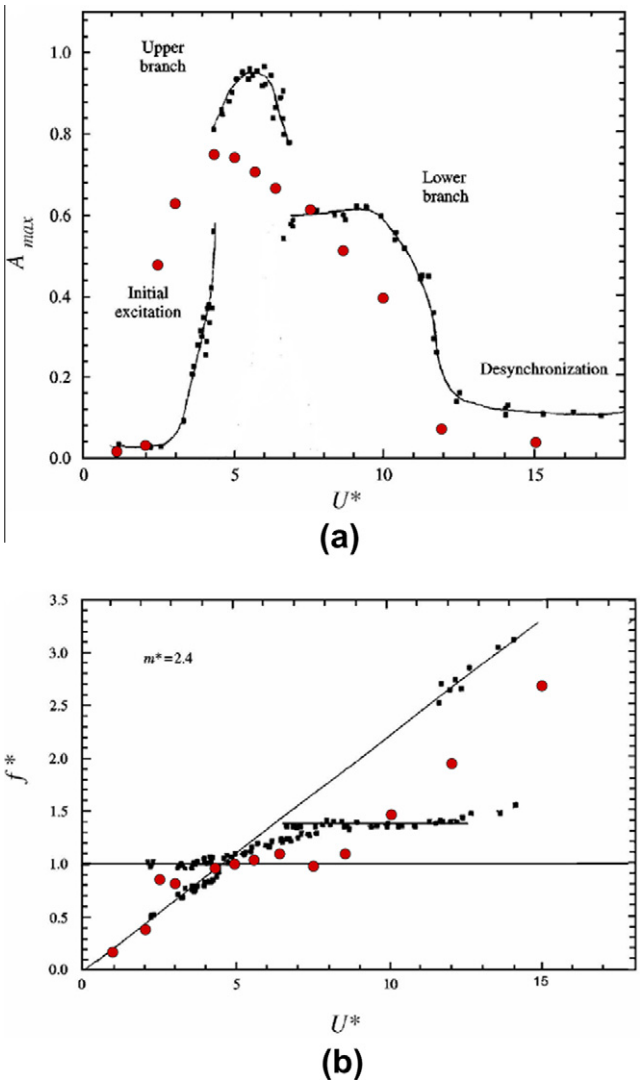

Fig. 9. Comparison of data from present study (circles) against Khalak and Williamson [17]. (a) A^* vs U^*, (b) f^* vs U^*.

Therefore, a simple numerical dye release method akin to an experimental ink shedding technique is implemented by solving $\frac{d\mathbf{X}_i}{dt} = \mathbf{u}_i, \forall i : 1 \ldots P$, along with the mass, momentum conservation equations. Here, particle positions and velocities are identified by $\mathbf{X}_i$ and $\mathbf{u}_i$ respectively for all P particles released. Streakline visuals thus generated are depicted in Fig. 4, and validated against the experiments of Taneda [42]. The distinct feature here, is the gradual roll-up of shear layers at crests and troughs. It should be noted that all these shed eddies are mutually connected by a trail streakline which originates in the near wake. The experimental visual in Fig. 4 was indeed produced by the illumination of a sheet of light, through electrolytic precipitation of a white colloidal smoke. To further assess the near wake dynamics and chaotic scattering that persists in this region, a close-up view of the experimental visuals of Sommerer et al. [43] is depicted, against the present simulations in Fig. 5. The most important parameters of practical interest are the force coefficients along streamwise and cross stream directions (C_d, C_l) and normalized vortex shedding frequency known as Strouhal number (St). A comparison of these parameters is presented in Table 1. The lift and drag forces [37] are obtained by integrating the normal and tangential stresses which are due to pressure and velocity gradients as given below:

$$C_d(t) = \int_0^{2\pi} \bar{p}\cos\theta d\theta - \frac{2}{Re}\int_0^{2\pi} \frac{\partial \bar{u}}{\partial x}\cos\theta d\theta + \frac{1}{Re}\int_0^{2\pi}\left(\frac{\partial \bar{u}}{\partial y} + \frac{\partial \bar{v}}{\partial x}\right)\sin\theta d\theta, \tag{16}$$

$$C_l(t) = -\int_0^{2\pi} \bar{p}\sin\theta d\theta - \frac{1}{Re}\int_0^{2\pi}\left(\frac{\partial \bar{u}}{\partial y} + \frac{\partial \bar{v}}{\partial x}\right)\cos\theta d\theta + \frac{2}{Re}\int_0^{2\pi} \frac{\partial \bar{v}}{\partial y}\sin\theta d\theta. \tag{17}$$

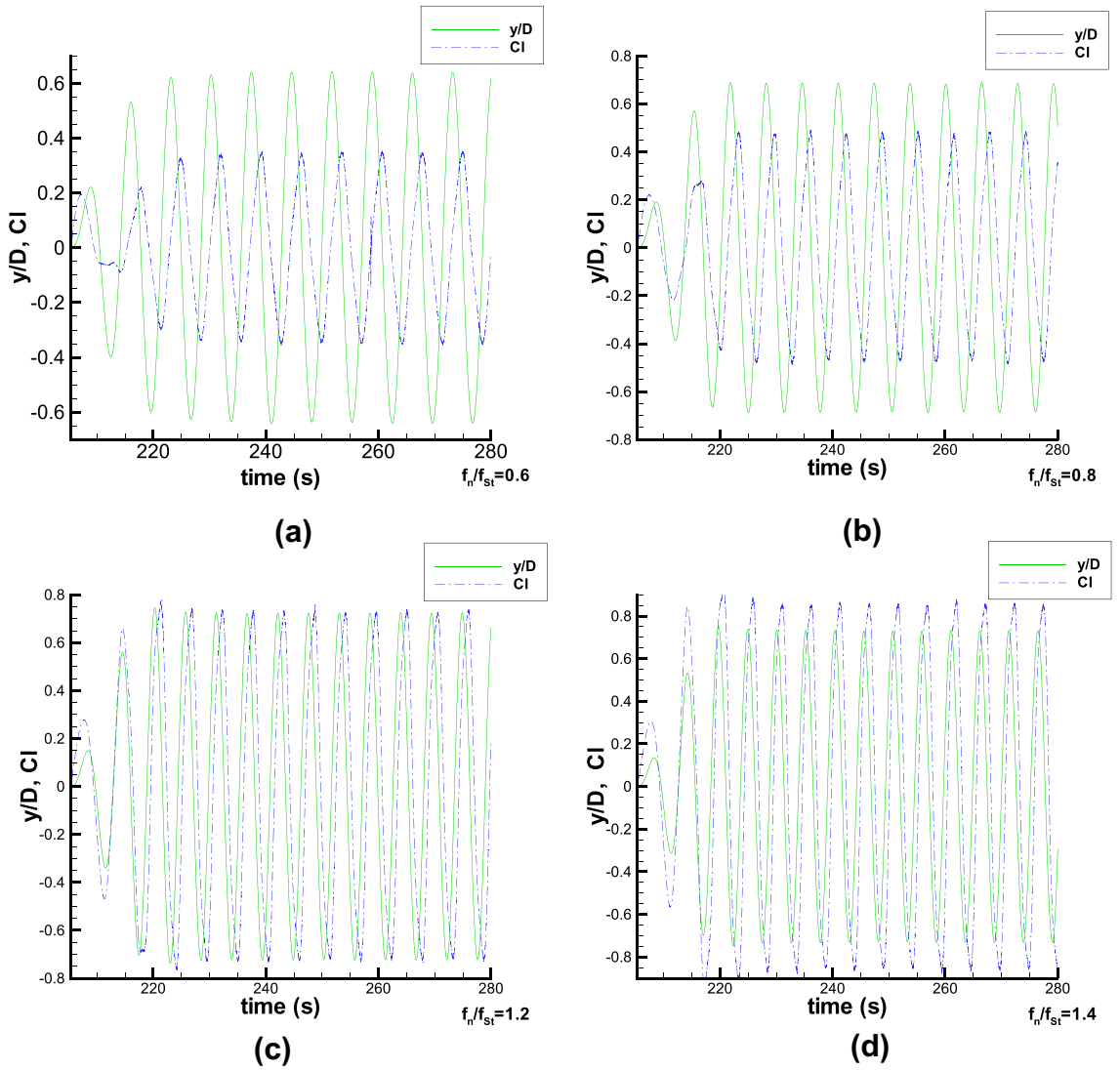

Fig. 10. Temporal history of lift force and displacement for different f_n/f_{St} and $m^* = 1.3$. (a) $f_n/f_{St} = 0.6$ (b) $f_n/f_{St} = 0.8$ (c) $f_n/f_{St} = 1.2$ and (d) $f_n/f_{St} = 1.4$.

Table 2
Grid sensitivity study to determine the amplitude of oscillation for $m^* = 1.3$.

Natural frequency (f_n)	Frequency ratio ($f^* = f_n/f_{St}$)	Grid (number of elements)			
		A (28884)	*B* (33350)	*C* (55844)	*D* (155158)
0.129	0.77	0.66	0.64	0.64	0.64
0.149	0.89	0.71	0.69	0.69	0.69
0.184	1.10	0.76	0.73	0.73	0.72
0.198	1.18	0.76	0.74	0.73	0.73

Here, θ refers to angle made with reference to the upstream vector and measured in a clock-wise sense. Further, *Re* refers to the Reynolds number $\left(\frac{\rho U_\infty D}{\mu}\right)$.

The fluctuating nature of the lift and drag forces can be seen in Fig. 6 for *Re* = 100. The actual design parameters of interest such as RMS lift and mean drag coefficient can be deduced from these temporal lift and drag coefficient histories respectively. Normalized vortex shedding frequency and hence the Strouhal number (*St*) were obtained by an FFT routine from the temporal lift force signals. Coefficient of drag and Strouhal number are defined as follows:

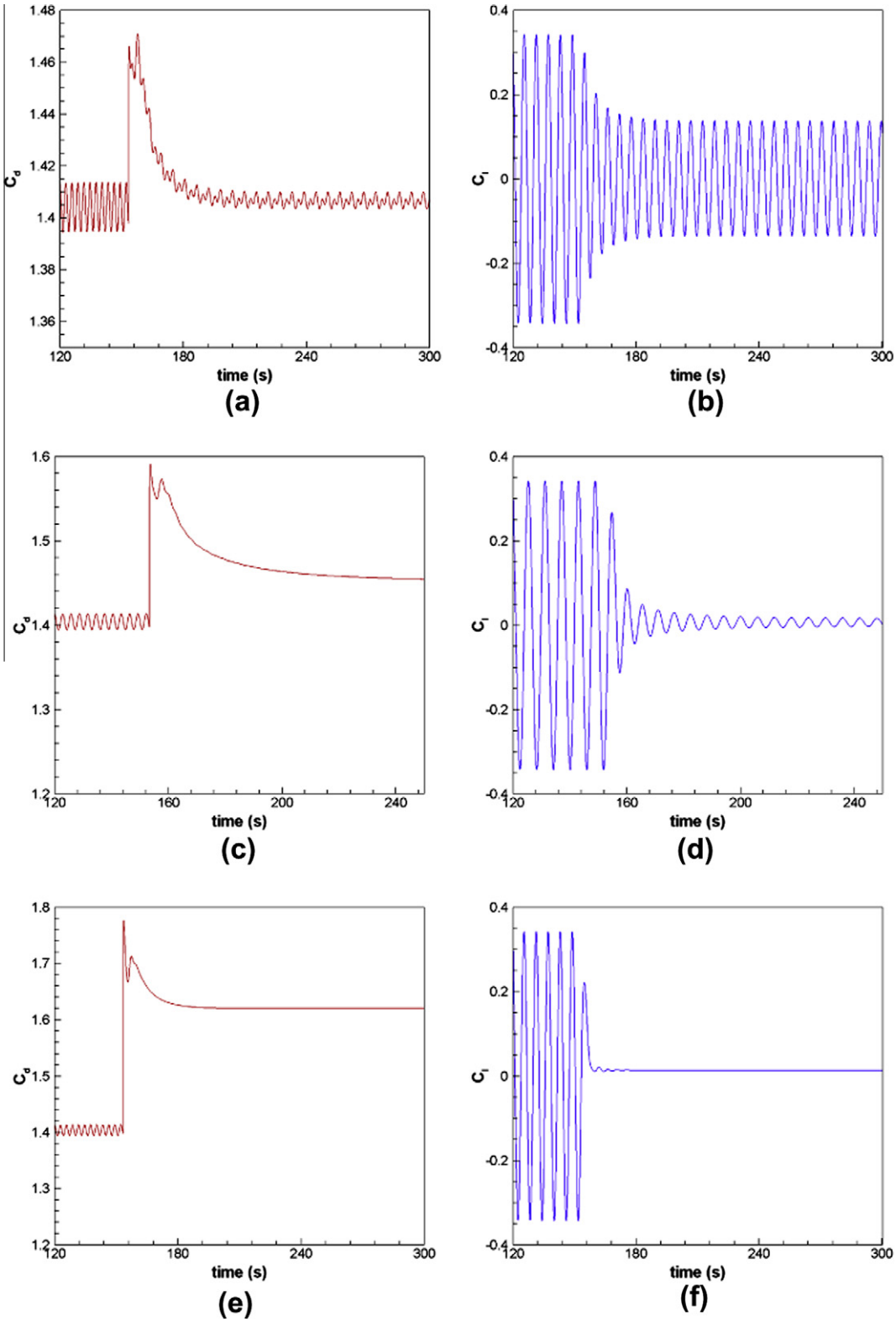

Fig. 11. C_d and C_l histories for 3 actuator control of flow past a fixed cylinder. (a-b) $U_{act}/U_\infty = 1.0$, (c-d) $U_{act}/U_\infty = 2.0$ and (e-f) $U_{act}/U_\infty = 3.0$.

Table 3
Effect of suction and blowing on the horizontal and vertical force coefficients on the circular cylinder.

$\xi = U_{act}/U_\infty$	$\overline{C}_d$	$C_{l,rms}(\overline{C}_l)$
1	1.41	0.097
2	1.46	0.008
3	1.62	0

Table 4
Flow control for a cylinder undergoing vortex induced vibrations $m^* = 1.3$, $f_n/f_{St} = 0.8$.

Control scheme used	$\overline{C}_d$	$C_{l,rms}$	A^*
No control applied	1.89	0.271	0.66
$U_{act}/U_\infty = 1$	1.65	0.267	0.6
$U_{act}/U_\infty = 2$	1.537	0.123	0.16
$U_{act}/U_\infty = 3$	1.64	0.008	0.003

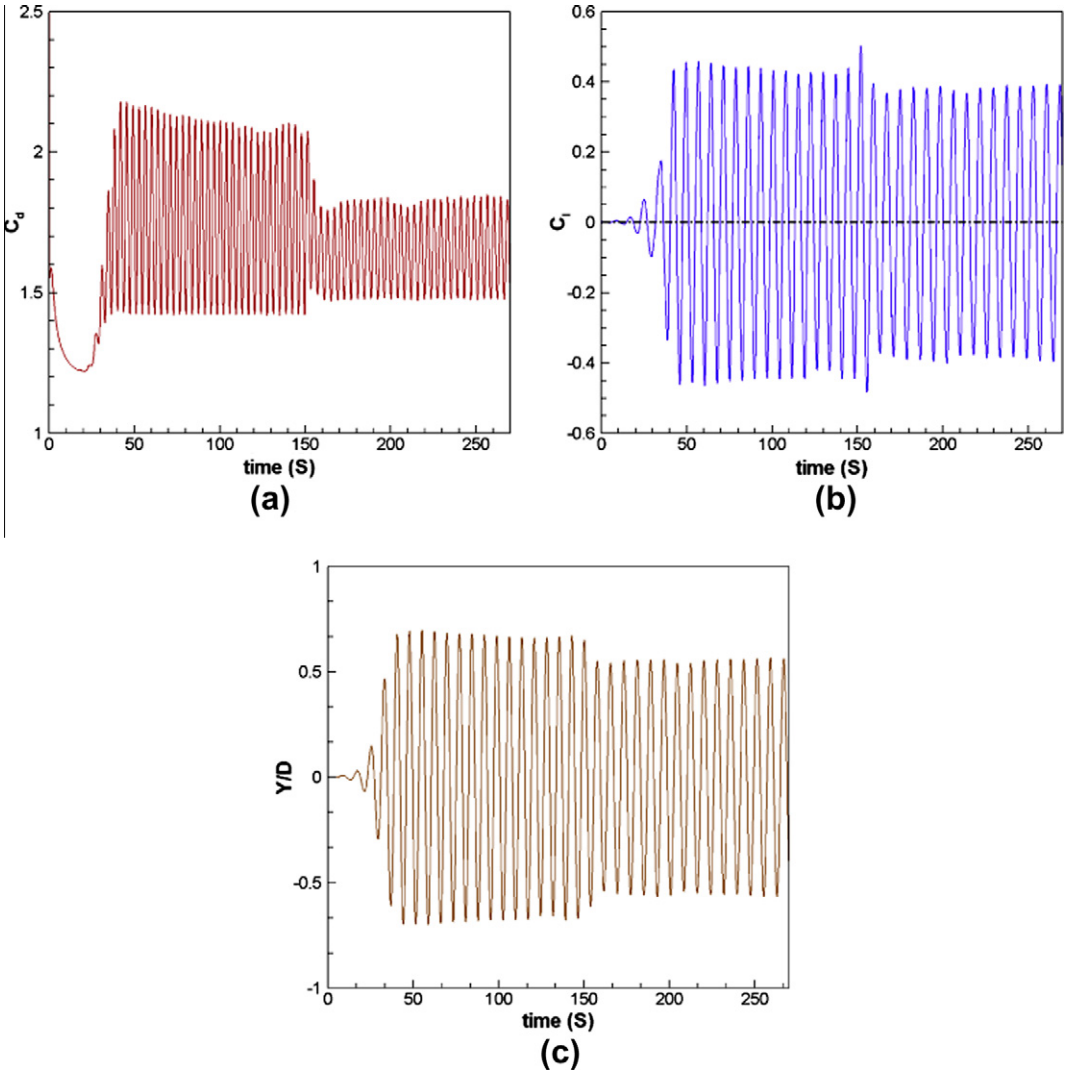

Fig. 12. C_d, C_l and cylinder displacement histories for 3 actuator control with $U_{act}/U_\infty = 1$. (a) C_d history, (b) C_l history, (c) position trace of centre of the cylinder.

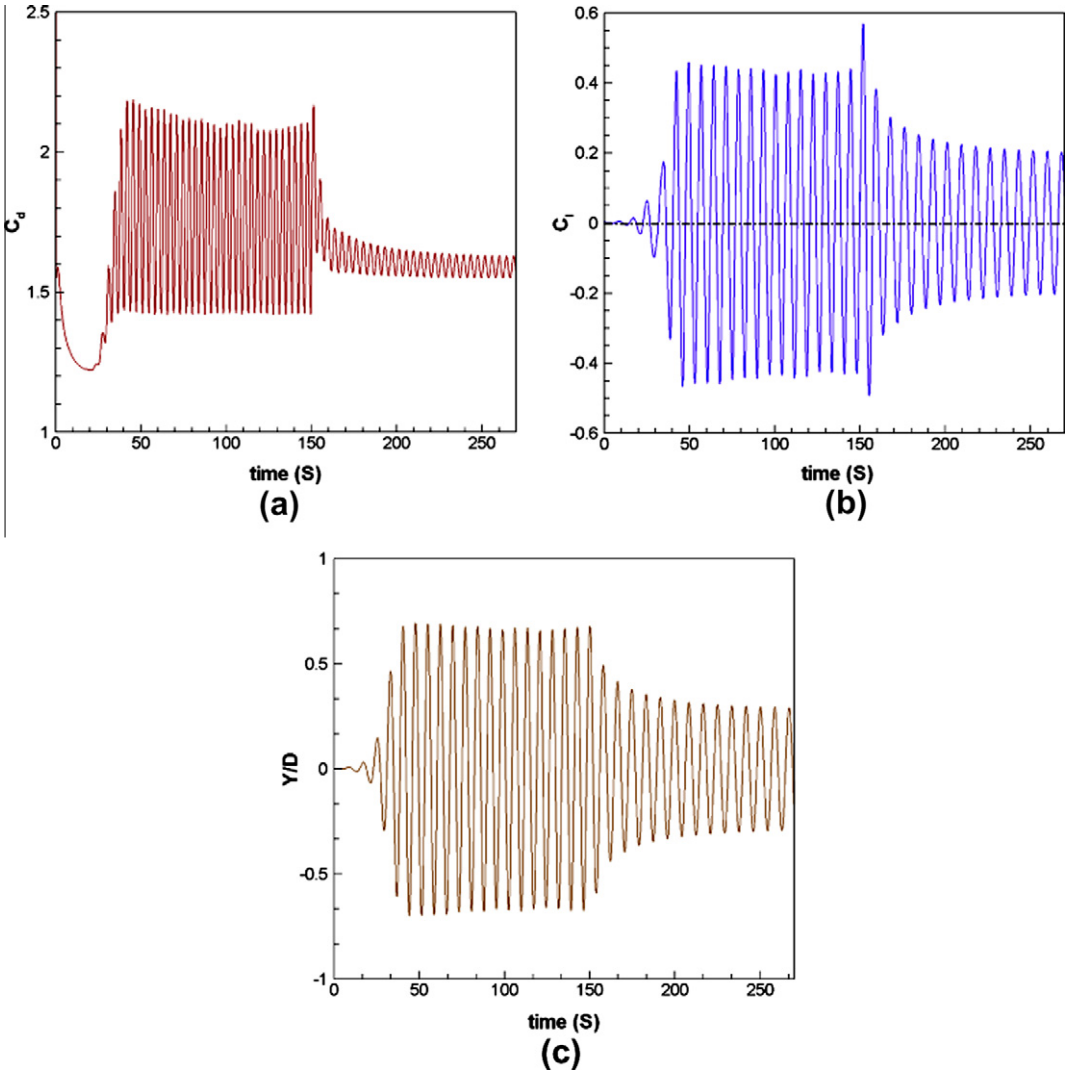

Fig. 13. C_d, C_l and cylinder displacement for 3 actuator control with $U_{act}/U_\infty = 2$. (a) C_d history, (b) C_l history, (c) Position trace of the centre of the cylinder (y/D).

$$\overline{C}_d = \frac{\overline{F}_D}{\frac{1}{2}\rho U_\infty^2}; \quad St = \frac{f_{vs}D}{U_\infty}, \tag{18}$$

where $\overline{F}_D$ is the time averaged mean drag force per unit area and f_{vs} is the vortex shedding frequency. From other experimental and numerical investigations, it can be noticed that, these parameters vary over a small range of values. Among these predictions, lift force fluctuations do not agree that well, compared to $\overline{C}_d$ and St. A similar view has been expressed by Sarpkaya [5] in his authoritative review on vortex induced vibrations.

3.2. Wake modifications under forced excitation

To study vortex induced vibrations, two distinct schools of thought are often employed. One is forced vibrations and other is free vibrations. In the context of forced vibrations, both amplitude and frequency of oscillation are chosen at will and superimposed on the structure. The influence of these vibrations on the wake vortices is often easier to categorize. This would also generate a wide repository of vortex structures which may/ may not be possible under self excited free vibrations. Nevertheless, in terms of numerical testing, this would enable validation of dynamic meshing capability. To this end, flow past a circular cylinder with external excitation is numerically investigated, where the coupling between the flow field and structural oscillations is unidirectional. Here cylinder displacements are imposed and do not have a bearing on the actual force exerted by the fluid. The motion of a the cylinder is idealized as, $y = A\sin(\omega t)$, where, A is the maximum amplitude of

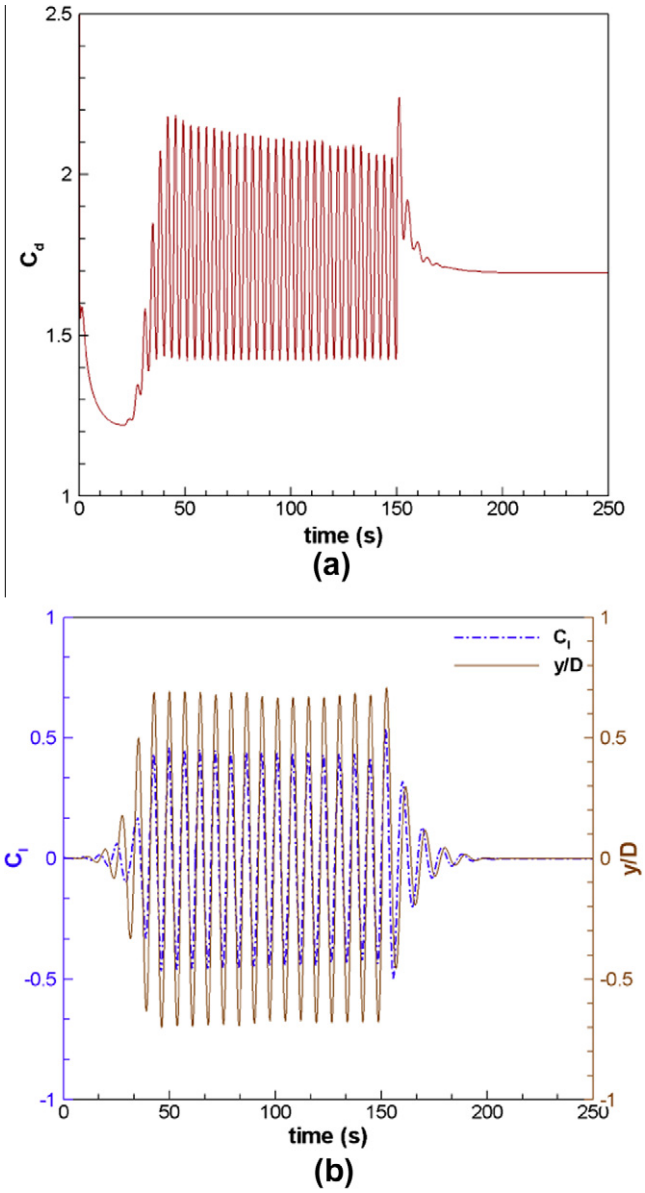

Fig. 14. C_d, C_l and cylinder displacement which depict phase difference plot for 3 actuator control with $U_{act}/U_\infty = 3$. (a) C_d history, (b) phase difference between C_l and y/D.

oscillation and ω refers to the imposed circular excitation frequency on the structure. The fluid flow patterns in the wake region are validated for different values of frequency–amplitude combinations. By conducting comprehensive experimental flow visualization studies, Williamson and Roshko [8] have generated a flow regime map by analyzing the wake patterns. Their experiments were in the *Re* range of 300–1000. The following amplitude and frequency combinations were chosen, to investigate the flow patterns behind the cylinder. (i) $A^* = 1$ and $f^* = 0.9$ to identify 2*P* like wake pattern. (ii) $A^* = 1.25$ and $f^* = 1.5$ to simulate *P* + *S* type pattern in the wake region. Here, the amplitude of oscillation (A^*) is normalized with cylinder diameter and cylinder excitation frequency with the Strouhal frequency (f_{St}). Results from the present investigation are compared with those obtained by Placzek et al. [31], in Figs. 7 and 8. Fig. 7 is of particular interest as it is neither a simple 2*S* nor a 2*P* pattern, although it can be thought of as a 'deformed' 2*S* mode.

3.3. Flow past a flexibly mounted circular cylinder

A circular cylinder mounted on flexible supports is an apt model to simulate free vibrations. These oscillations are triggered by the fluid forces, which in turn determine the motion of the cylinder. Here, a dynamical evolution equation which

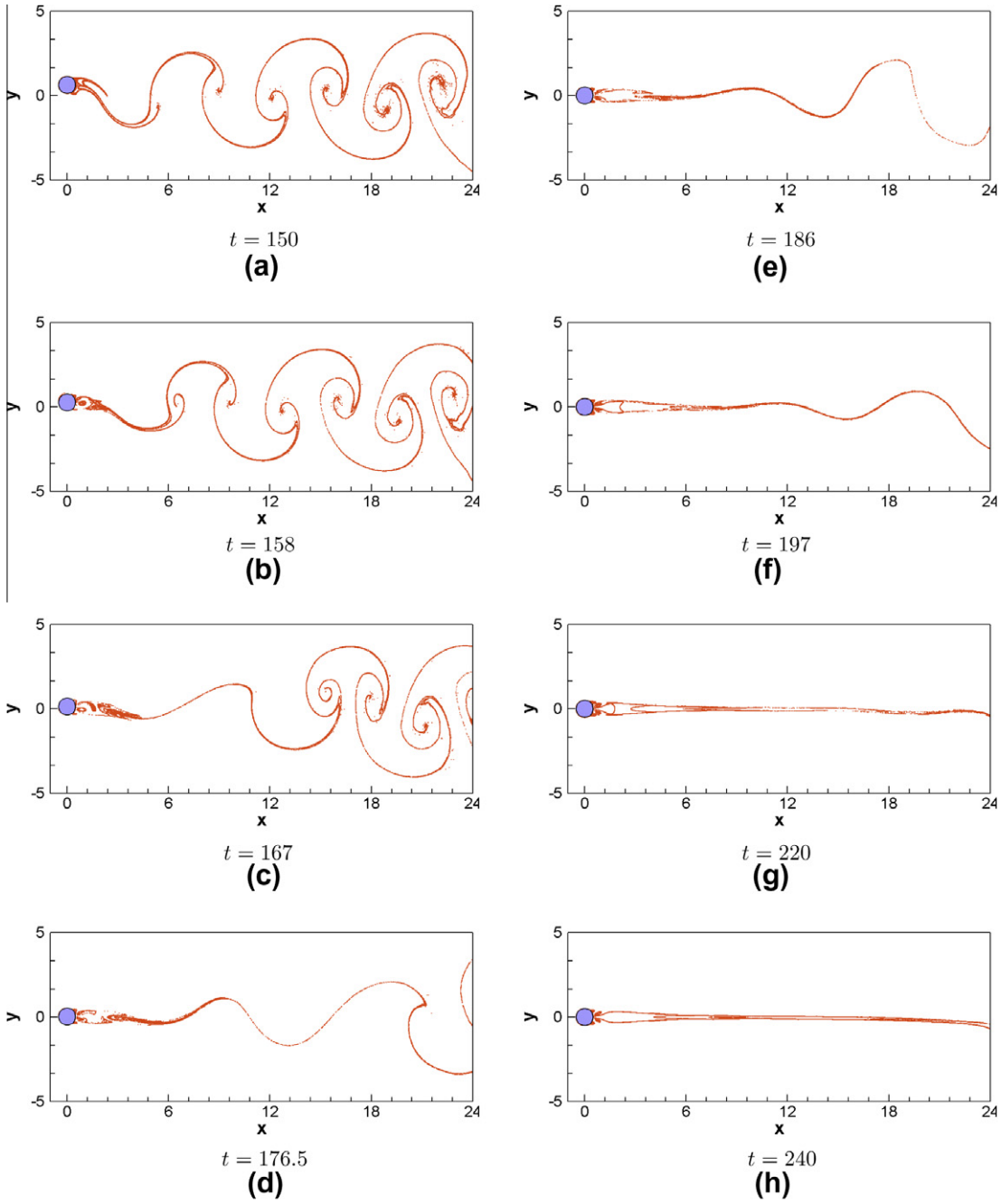

Fig. 15. Temporal evolution of the streakline patterns and its wake control for $U_{act}/U_{\infty} = 3.0$. Note in particular, gradual annihilation of wake vortices and its attendant suppression of flow induced oscillations.

governs the motion of the structure needs to be solved. A spring-mass-damper system idealizes the structural oscillations reasonably well. To this end, equation of structure (Eq. (1)) is solved after evaluating fluid forces acting on the surface of the cylinder. The mass ratio (m^*) defined as $m/\rho D^2$ is chosen as 2.4, similar to earlier studies to enable comparison against the findings of Khalak and Williamson [17], at different ratios of $f^* = f_n/f_{St}$. It should be noted that, although the synchronization region is rather broad, it conforms with the experimental results, shown in Fig. 9. The present study agrees well with the findings of Khalak and Williamson [17] as far as the broad trends of desynchronization, the presence of upper and lower branches and response frequency variation, etc. are concerned. However, unlike experiments, numerical simulations can be performed only at discrete values of reduced velocity U^* to determine the peak amplitude of oscillation. Increase or decrease of U^* is naturally achieved in experiments by slowly varying the in flow velocity. However, in numerics the hysteresis effects that are visible in the experiments can not be easily replicated.

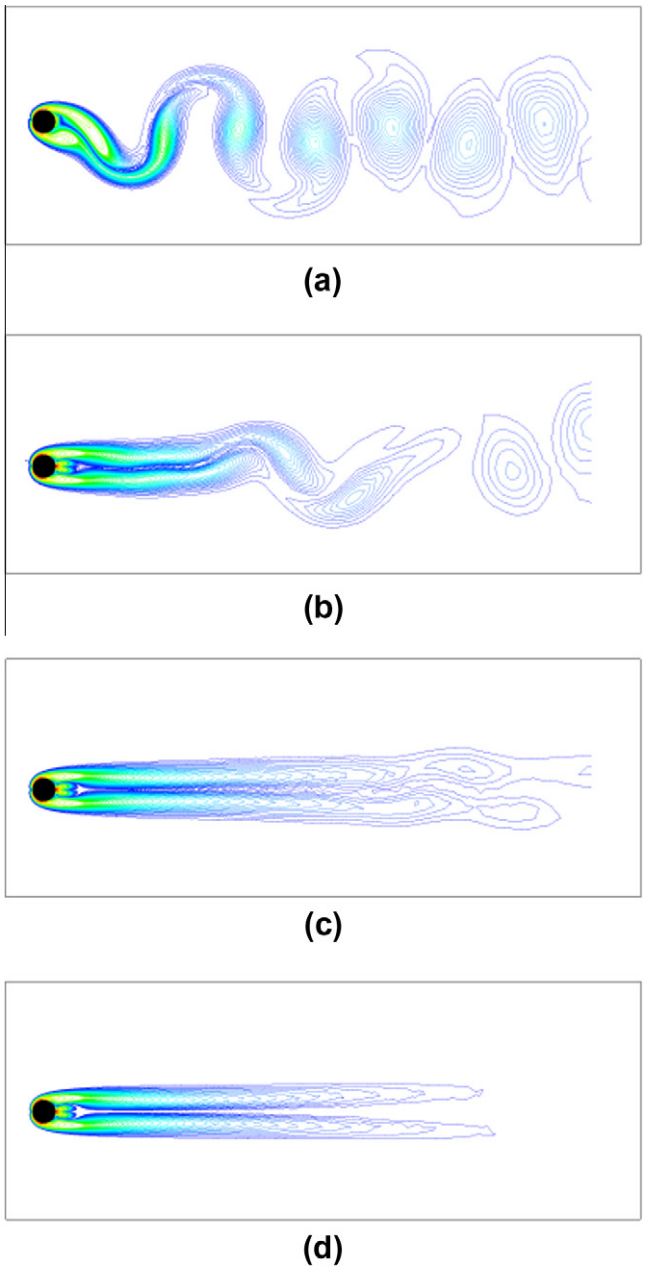

Fig. 16. Temporal evolution of vorticity contours at discrete time levels during the actuation process when control parameter is 3.0. (a) $t = 150$, (b) $t = 167$, (c) $t = 197$, (d) $t = 220$.

A lower mass ratio $m^* = 1.3$ is chosen for subsequent studies as low mass damping implies higher amplitude of oscillations. For such cases, it is possible to build a quick response system, when a new control strategy is to be tested. The two way coupling that exemplifies the interaction between the fluid and structure can be best observed through the temporal lift history plots overlayed with maximum amplitude of oscillation as in Fig. 10. A grid sensitivity study was carried out to ensure that the results are not influenced by the fineness of the grid. Different grid sizes employed and their corresponding maximum amplitude of oscillation are presented in Table 2. It is observed that the values of transverse oscillations do not significantly differ between fine and finer meshes.

3.4. Flow control using three actuator system

In the present investigation a three actuator system is designed, which consists of a blowing slot and two suction slots on the cylinder surface. For the implementation of flow control, actuator locations are identified on either side (see Fig. 1). These

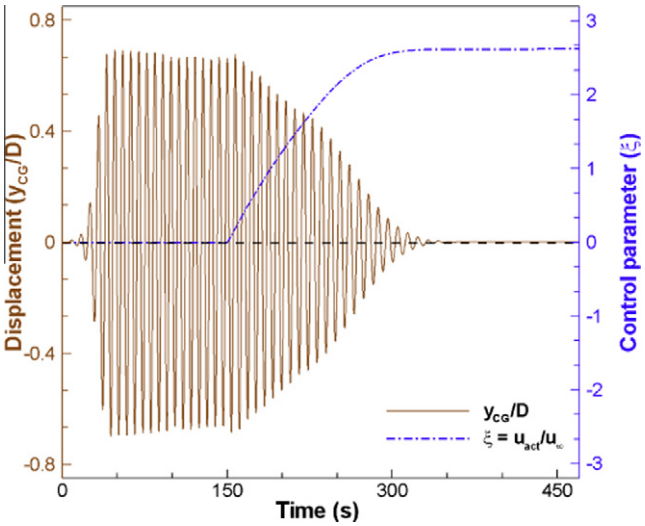

Fig. 17. Gradual suppression of free vibrations, when control was switched on at $t = 150$. The control input reaches a dynamically steady value. The dynamic adaptability of the present control strategy is tested.

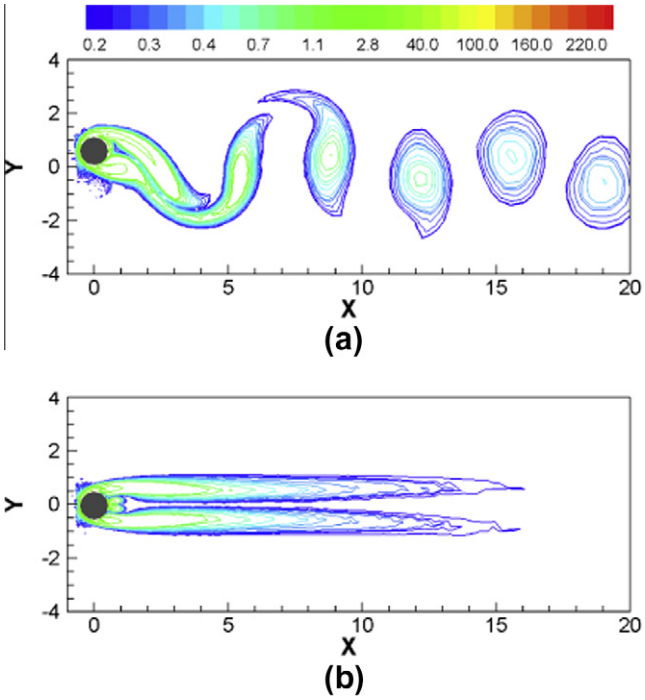

Fig. 18. Wake patterns (a) before control at $t = 150$, (b) after control at $t = 450$.

surfaces are assigned a *mass flow* boundary condition to enable suction with zero net mass injection. This is achieved by means of a single blowing slot at the rear stagnation point as indicated in the figure.

3.4.1. Control of vortex shedding behind a rigid cylinder

To start with, the three actuator system is evaluated for its effectiveness in suppressing vortex shedding past a fixed cylinder. It is found that, for low values of U_{act}/U_∞ a marked reduction in $C_{l,rms}$ was achived. For higher values of U_{act}/U_∞, the vortex shedding is completely suppressed, albeit with a significant drag penalty. The lift and drag histories for the three cases are shown in Fig. 11. Corresponding $\overline{C}_d$ and $C_{l,rms}$ are presented in Table 3. The trade-off is that the drag force (measured through C_d) increases by about 15–20%. If the objective is to control flow induced vibrations, the three actuator system appears to be a reasonable choice, although the energy expenditure for its implementation has to be accounted.

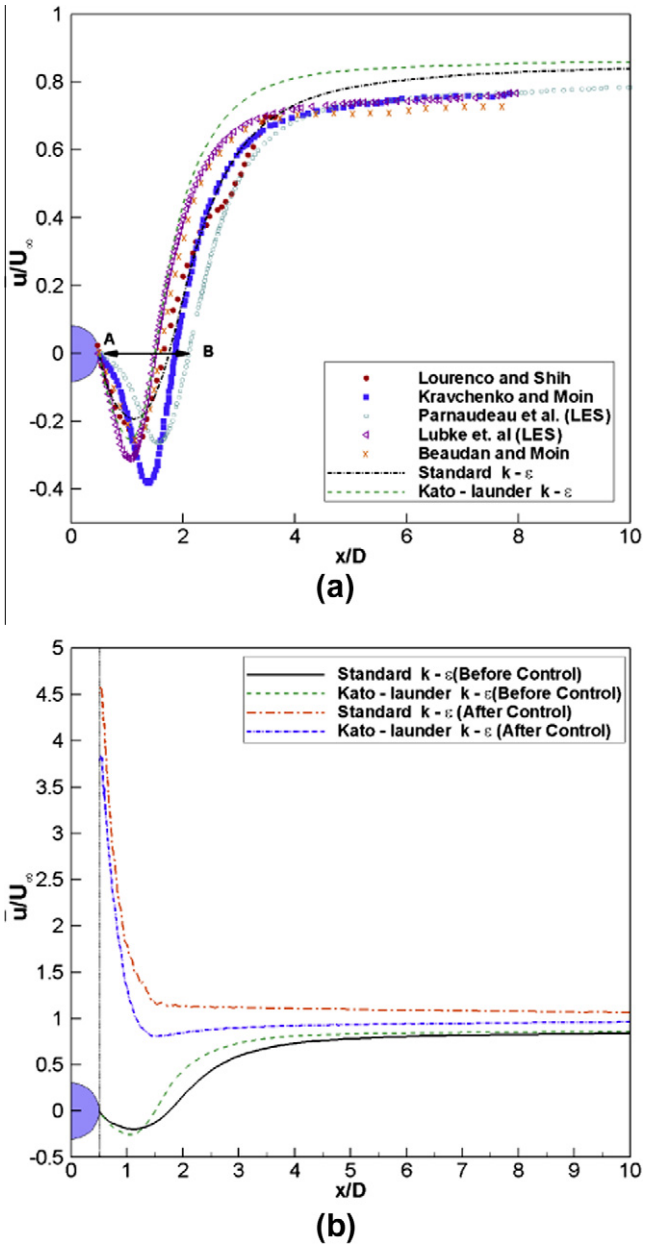

Fig. 19. Mean streamwise velocity along the wake center line for $Re = 3900$. (a) Validation with Lourenco and Shih [44], Kravchenko and Moin [45], Parnaudeau et al. [44], Lübcke et al. [46], Beaudan and Moin [46] and (b) before and after control.

3.4.2. Control of vortex induced vibrations of a flexibly mounted circular cylinder

For a circular cylinder undergoing free vibrations, the self excited motion is triggered by the lift force fluctuation. This would act as an excitation force in the generation of cylinder oscillations. Therefore, control of vortex induced vibrations for a 1DOF system would involve control of the lift force fluctuations, which need to be suppressed. Here, control goal is to obtain a reduction in $C_{l,rms}$ without being concerned about the drag penalty. The proposed three actuator system does reduce the RMS lift and therefore, qualifies to perform well for the suppression of flow induced vibration.

To further investigate the efficacy of the three actuator system, self excited oscillations are allowed to manifest. This would enable the cylinder to move freely until it reaches its full blown form of steady periodic oscillations. A fixed quantum of suction-blowing is invoked at an arbitrary set point $(t = 150)$ after periodic cylinder oscillations were clearly established. Since there is no periodicity associated with the control, the exact point of actuation is not very important. The results of the present investigation are shown in Table 4, and the temporal histories of drag and lift coefficient fluctuations are shown in Figs. 12–14. Applying a lower quantum of predetermined input $\left(\frac{U_{act}}{U_\infty}\right)$ is able to reduce the wake width. However, complete

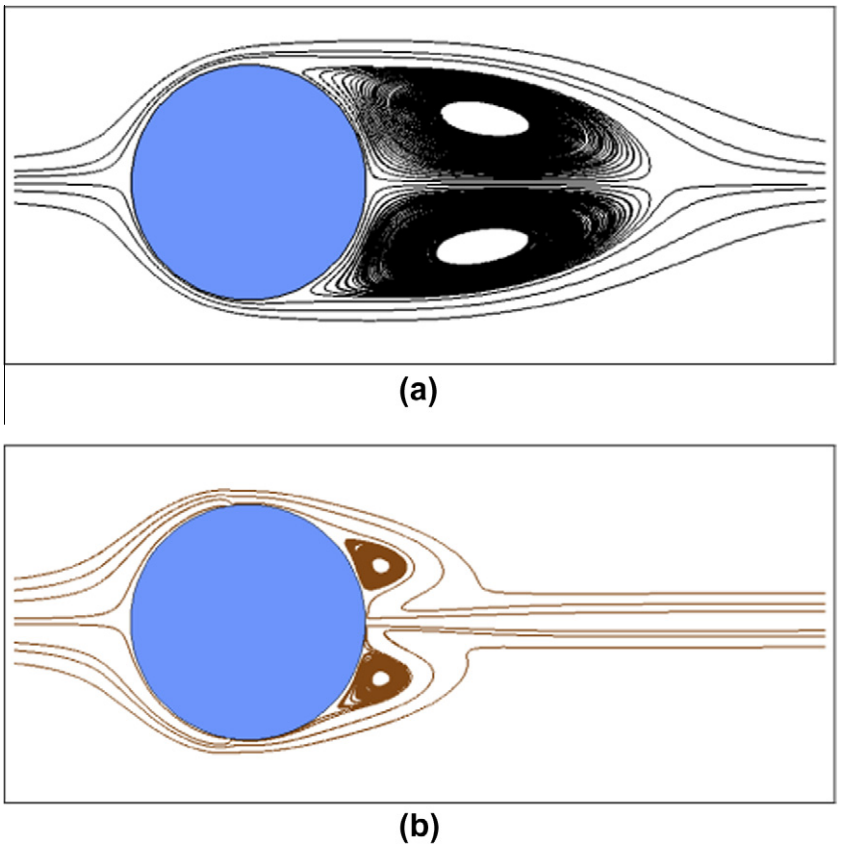

Fig. 20. Time averaged streamlines in the wake behind the main circular cylinder with standard $k-\epsilon$ model at $Re = 3900$. (a) without control and (b) with control.

suppression of either vortex street formation or the cylinder oscillations was not possible. All the parameters of interest show a small reduction, but not significant enough to justify the control input in implementing this strategy. The reduction in cylinder oscillation amplitude is significant as we increase the quantum of control. The scheme with $U_{act}/U_{\infty} = 3.0$ completely suppresses the vibrations. This system further settles close to a state of zero lift force fluctuation. Streakline visuals are generated under the influence of suction and blowing as shown in Fig. 15 at different time levels. The self excited cylinder vibrations are automatically controlled with the right quantum of actuator input as shown in Fig. 15(f). Furthermore, the temporal evolution of the vorticity contours for $U_{act}/U_{\infty} = 3.0$ are depicted in Fig. 16. Complete vortex shedding suppression could be achieved with a holistic control on the absolute instability zone. This zone exemplifies the origin of instabilities and their growth right behind the cylinder. However, during temporal evolution, convective instability region persists, as reflected through the downstream convection of vortices, although absolute instability region is under control. A completely quiescent wake zone was achieved at $t = 220$.

3.4.3. Dynamic adaptability of control by suction and blowing

To investigate the dynamic nature of the vortex induced oscillations and its suppression, a sensitivity check is carried out by designing a simple proportional controller as suggested in Refs. [26,27]. This control equation is implemented along with the equation of structure and solved with mass and momentum conservation equations for the fluid motion. If the actuation parameter (ξ) is defined as the ratio of velocity of blowing (or) suction to the free stream velocity $\left(\frac{U_{act}(t)}{U_{\infty}}\right)$, the dynamical evolution of ξ is given as:

$$\frac{d\xi(t)_{a_i}}{dt} = C\sigma(t). \tag{19}$$

In the above equation, a_i, refers to the actuation slots, which enable either suction or base bleed. $\sigma(t)$, refers to the maximum standard deviation against time in each cycle of oscillation, which is given as:

$$\sigma(t) = \max|y_{CG}(t) - \tilde{y}_{CG}(t)|, \tag{20}$$

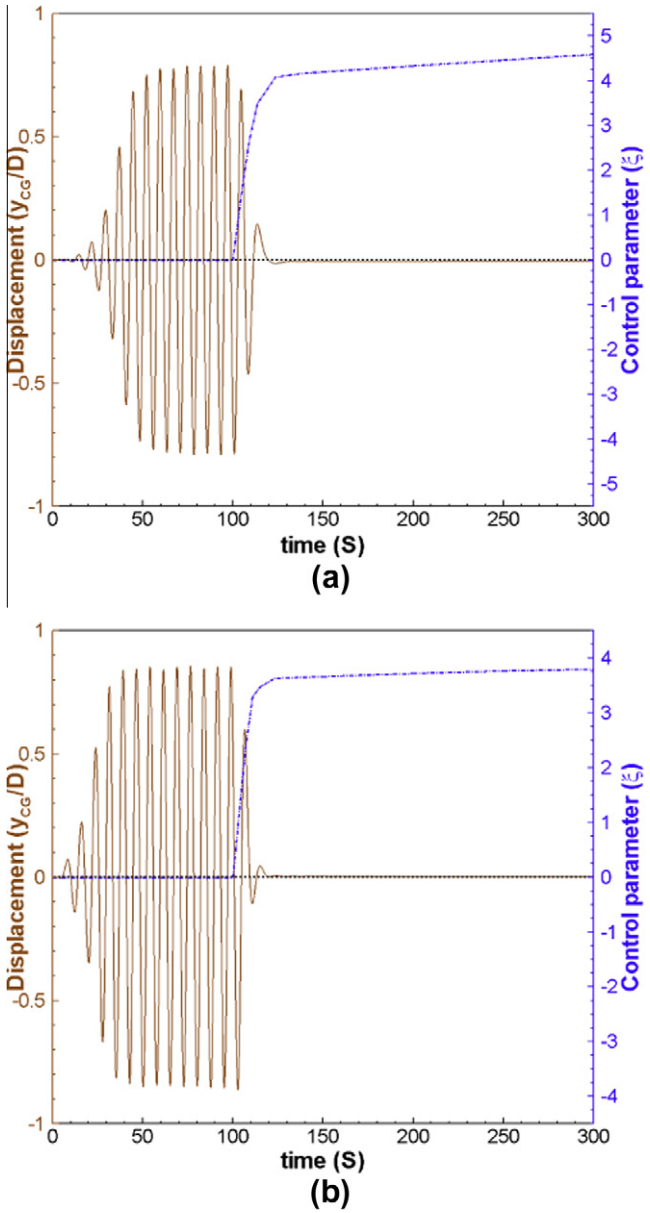

Fig. 21. Gradual suppression of free vibrations at $Re = 3900$, when control was switched on at $t = 100$. The control input reaches a dynamically steady value. (a) standard $k - \epsilon$ and (b) $k - \epsilon$ of Kato-Launder.

where y_{CG} denotes the position of the centre of gravity of the vibrating cylinder about its desired equilibrium position $\tilde{y}_{CG}$, which is free from oscillations. The control Eq. (19) described above is a generic one that determines the actuation parameter, which is implemented as a user defined function (UDF) and is evolved simultaneously with the Navier–Stokes calculations. Here, the coefficient C is the proportionality constant and can be varied like a fuzz factor. This set of coupled equations render an opportunity to monitor the gradual suppression of cylinder oscillation as shown in Fig. 17 and 18. The complete annihilation of wake vortices can be noticed when the control input reaches steady state. Interestingly, a value of $\xi = 2.6$ obtained through dynamic adaptivity, is close to the a value 3.0 predicted by the predetermined controller input.

3.4.4. Influence of suction and blowing control on the turbulent wake

At Reynolds number 3900 the wake is fully turbulent, although the boundary layer is laminar. Resolving features of the turbulent fluctuations in the wake region by URANS approach is limited by the approximation capability of the turbulent eddy viscosity hypothesis employed for the Reynolds stress tensor. If physics of the anisotropic nature of vortex shedding could be captured through these models, the features could be better resolved. So, the acuracy of these turbulence models

in predicting the forces and flow parameters influence (i) the calculation of structural oscillations and (ii) the efficacy of suction-blowing control.

In the present study, the control equation and the governing equation of the structure are coupled and solved simultaneously along with a chosen two equation turbulence model. The time averaged mean and turbulence characteristics are obtained over ten vortex shedding cycles, after reaching steady periodic state. The location of the centre of mean vortex and length of formation region (L_f) is quantified by plotting normalized mean streamwise velocity ($\bar{u}_{cl}$) against the wake centreline as shown in Fig. 19(a). The plot signifies the predictive capability of two models vis-á-vis other numerical and experimental investigations. The models tested have a better comparison with both PIV and LES data in the far wake region. However, there is a clear under prediction on the location of centre of mean vortex, length of the wake formation region (L_f) – as indicated by AB and the corresponding magnitude of velocity. The influence of suction-blowing control averaged over a long time period is shown in Fig. 19(b). Corresponding vortex formation length under the influence of adaptive control is shown in Fig. 20. Here, the streamline topology involves two large counter-rotating eddies in the near-wake region. However, under the influence of control the eddies get shrunk very close to the cylinder surface, indicating a tighter and a tiny wake formation region. Note in particular, the fluid is able to reach the rear stagnation point and contain the absolute instability region. This is a typical signature of the complete annihilation of wake vortices. Thus, flow induced oscillations are effectively controlled even for turbulent flow conditions as depicted in Fig. 21. Therefore, the coupled control strategy is found to be effective when τ_{ij}^R modelling is achieved either through standard $k-\epsilon$ or Kato-Launder $k-\epsilon$ models.

4. Summary and conclusions

Control of vortex structures behind a flexibly mounted cylinder is investigated for $Re = 100$. A three actuator system is designed to study the efficacy of controlling cylinder oscillations. For the purpose of validation, flow past a circular cylinder is numerically simulated under 3 specific cases viz.: (a) stationary cylinder, (b) rigid cylinder subject to forced excitations, (c) freely vibrating cylinder. The influence of either forced or free structural vibrations on the wake vortices behind the body is numerically investigated. Once the phenomena of self excited oscillations are captured, they are coupled with the suction-blowing strategy for enabling actuations on the vibrating structure. From this study, the following conclusions can be drawn:

- Flow past a rigid cylinder is validated for the lift and drag forces imparted on the cylinder and the Kármán shedding frequency, responsible for these force fluctuations.
- Study of flow past a cylinder under forced excitation produces some wake patterns not typically seen in free vibration studies. This is due to the fact that, in forced vibrations, the amplitude and frequency of oscillation of the cylinder are not coupled to influence the flow field. For flow in the laminar regime at $Re = 100$, the deformed $2S$ and $P+S$ vortex formation modes are numerically validated.
- Flow past a flexibly mounted cylinder and its effect on the wake zone was studied for $Re = 100$, and as expected, it was found that the drag and lift forces increase substantially when the cylinder is allowed to vibrate. The mass-spring-damper system was found to produce results that compare well with the available literature for similar mass ratios.
- The three actuator system, which comprises of two suction slots and a blowing slot, was found to be remarkably effective in suppressing vortex induced oscillations. For higher quantum of actuation ($U_{act}/U_\infty \geqslant 3.0$), the lift fluctuations were found to be completely suppressed.
- The dynamic adaptability of the present actuator system is further validated by designing a control equation and coupling the same with the governing equations. It was noticed that, for $U_{act}/U_\infty \approx 2.6$, complete suppression of vortex induced oscillations could be achieved. This value is remarkably close to $U_{act}/U_\infty = 3.0$, when simulations were performed under predetermined actuator inputs.
- At high Reynolds numbers, even the turbulent wake structures could be suppressed through the proposed control strategy. For $Re = 3900$, the wake formation length is effectively zero indicating complete suppression of vortex shedding and attendant flow induced oscillations.

It should be mentioned that, in the present simulations, self excited oscillations were first allowed to be generated up to their steady periodic full blown form, before the control was initiated. It should further be noted that the control for a cylinder with very low mass damping, which generates high amplitudes of oscillation is successfully predicted. Low mass damping cases are typically the flow of water past a body. So these strategies can be thought of as effective approaches for structures under ocean engineering settings. For high mass damping cases, typically flows involving air, the amplitudes would be lower, so the quantum of control needed for suppressing the oscillations would probably be less.

References

[1] M.M. Zdravkovich, Flow Around Circular Cylinders, Fundamentals, vol. 1, OUP, New York, 1997.
[2] R.D. Blevins, Flow Induced Vibrations, Von Nostrand Reinhold, New York, 1990.
[3] R. Goverdhan, C.H.K. Williamson, Vortex induced vibrations, Annu. Rev. Fluid Mech. 36 (2004) 413–455.
[4] R.D. Gabbai, H. Benaroya, An overview of modeling and experiments of vortex-induced vibration of circular cylinders, J. Sound Vib. 282 (2005) 575–616.
[5] T. Sarpkaya, A critical review of the intrinsic nature of vortex-induced vibrations, J. Fluid Struct. 19 (2004) 389–447.

[6] G.H. Koopman, The vortex wakes of vibrating cylinders at low Reynolds numbers, J. Fluid Mech. 28 (1967) 501–512.
[7] R.E.D. Bishop, A.Y. Hassan, The lift and drag forces on a circular cylinder oscillating in a flowing fluid, Proc. R. Soc. Lond. Ser. A 227 (1964) 51–75.
[8] C.H.K. Williamson, A. Roshko, Vortex formation in the wake of an oscillating cylinder, J. Fluid Struct. 2 (1988) 355–381.
[9] C.C. Feng, The Measurement of Vortex Induced Effects in Flow Past Stationary and Oscillating Circular and D-section Cylinders, The University of British Columbia, Canada, 1968.
[10] P. Anagnostopoulos, P.W. Bearman, Response characteristics of a vortex-excited cylinder at low Reynolds numbers, J. Fluid Struct. 6 (1992) 39–50.
[11] S.E. Hurlbut, M.L. Spaulding, F.M. White, Numerical solution for a laminar two dimensional flow about a cylinder oscillating in a uniform stream, J. Fluid Eng. 104 (1982) 104–120.
[12] R. Chilikuri, Incompressible laminar flow past a transversely vibrating cylinder, J. Fluid Eng. 109 (1987) 166–171.
[13] B.S.V. Patnaik, P.A.A. Narayana, K.N. Seetharamu, Numerical simulation of laminar flow past a transversely vibrating circular cylinder, J. Sound Vib. 288 (3) (1999) 459–475.
[14] J.R. Meneghini, P.W. Bearman, Numerical simulation of high amplitude oscillatory flow about a circular cylinder, J. Fluid Struct. 9 (1995) 435–455.
[15] C.Y. Zhou, C. Sorm, K. Lam, Vortex induced vibrations of an elastic circular cylinder, J. Fluid Struct. 13 (1999) 165–189.
[16] T.S. Leontini, B.E. Stewart, M.C. Thompson, K. Hourigan, Predicting vortex-induced vibrations from driven oscillation results, Appl. Math. Model. 30 (2006) 1096–1102.
[17] A. Khalak, C.H.K. Williamson, Investigation of the relative effects of mass and damping in vortex induced vibration of a circular cylinder, J. Wind Eng. Ind. Aerodyn. 69–71 (1997) 341–350.
[18] V.J. Modi, Moving surface boundary-layer control: a review, J. Fluid Struct. 11 (1997) 627–663.
[19] A.R. Kumar, S. Chan-Hyun, B.H.L. Gowda, Passive control of vortex-induced vibrations: an overview, Recent Patents Mech. Eng. 1 (2008) 1–11.
[20] H. Baek, G.E. Karniadakis, Suppressing vortex-induced vibrations via passive means, J. Fluid Struct. 25 (2009) 848–866.
[21] Z. Chen, N. Aubry, Closed-loop control of vortex-induced vibration, Commun. Nonlinear Sci. Numer. Simul. 10 (2005) 287–297.
[22] Z. Li, I.M. Navon, M.Y. Hussaini, F.-X. Le Dimet, Optimal control of cylinder wakes via suction and blowing, Comput. Fluids. 32 (2003) 149–171.
[23] N. Fujisawa, G. Takeda, Flow control around a circular cylinder by internal acoustic excitation, J. Fluid Struct. 17 (2003) 903–913.
[24] P.T. Tokumaru, P.E. Dimotakis, Rotary oscillation control of a cylinder wake, J. Fluid Mech. 224 (1991) 77–90.
[25] E. Ott, C. Grebogi, J.A. Yorke, Controlling chaos, Phys. Rev. Lett. 64 (11) (1990) 1196–1199.
[26] B.S.V. Patnaik, G.W. Wei, Controlling wake turbulence, Phys. Rev. Lett. 88 (2002) 054502.
[27] S. Muddada, B.S.V. Patnaik, An active flow control strategy for the suppression of vortex structures behind a circular cylinder, Eur. J. Mech. B. Fluids 29 (2010) 93–104.
[28] C.H.K. Williamson, Vortex dynamics in the cylinder wake, Annu. Rev. Fluid Mech. 28 (1996) 477–539.
[29] S.V. Patankar, Numerical Heat Transfer and Fluid Flow, Hemisphere, Washington, DC, 1980.
[30] Fluent 6.2, User's Guide, Fluent Inc., 2006.
[31] A. Placzek, S. Jean-François, A. Hamdouni, Numerical simulation of an oscillating cylinder in a cross-flow at low Reynolds number: forced and free oscillations, Comput. Fluids 38 (2009) 80–100.
[32] H.J. Ferziger, M. Peric, Computational Methods for Fluid Dynamics, Springer, Berlin, 1999.
[33] P.A. Davidson, Turbulence: An Introduction for Scientists and Engineers, Oxford University Press, Great Clarendon Street, Oxford ox2 6DP, 2005.
[34] W. Rodi, Comparison of LES and RANS calculations of the flow around bluff bodies, J. Wind Eng. Ind. Aerodyn. 69 (1997) 55–75.
[35] B.E. Launder, D.B. Spalding, The numerical computation of turbulent flow, Comput. Methods Appl. Mech.Eng. 3 (1974) 269–289.
[36] B.E. Launder, B.I. Sharma, Application of the energy-dissipation model of turbulence to the calculation of flow near a spinning disc, Lett. Heat Mass Transfer 1 (1974) 131–138.
[37] Z.C. Zheng, N. Zhang, Frequency effects on lift and drag for flow past an oscillating cylinder, J. Fluid Struct. 24 (2008) 382–399.
[38] M.S. Engelman, Md-Ali Jamina, Transient flow past a circular cylinder: a bench mark solution, Int. J. Numer. Methods Fluids 11 (1990) 985–1000.
[39] S. Kang, H. Choi, S. Lee, Laminar flow past a rotating circular cylinder, Phys. Fluids 11 (1999) 3312–3321.
[40] B. Sharman, F.S. Lien, L. Davidson, C. Norberg, Numerical prediction of low Reynolds number flows over two tandem circular cylinders, Int. J. Numer. Methods Fluids 47 (2005) 427–447.
[41] A. Burbeau, P. Sagaut, Simulation of a viscous compressible flow past a circular cylinder with higher-order discontinuous Galerkin methods, Comput. Fluids 31 (2002) 887–889.
[42] M. Van Dyke, An Album of Fluid Motion, Parabolic Press, 1988.
[43] J.C. Sommerer, H.-C. Ku, H.E. Gilreath, Experimental evidence for chotaic scattering in a fluid wake, Phys. Rev. Lett. 77 (25) (1996) 5055–5058.
[44] P. Parnaudeau, J. Carlier, D. Heitz, E. Lamballais, Experimental and numerical studies of the flow over a circular cylinder at Reynolds number 3900, Phys. Fluids 20 (2008) 085101.
[45] A.G. Kravchenko, P. Moin, Numerical studies of flow over a circular cylinder at $Re_D = 3900$, Phys. Fluids 12 (2) (2000) 403–417.
[46] H. Lübcke, St. Schmidt, T. Rung, F. Thiele, Comparison of LES and RANS in bluff-body flows, J. Wind Eng. Ind. Aerodyn. 89 (2001) 1471–1485.